# Validation of a Two-Phase CFD Model for Predicting Propellant Tank Pressurization and Pressure Collapse in The Ground-Based K-Site Hydrogen Slosh Experiment

Olga Kartuzova[1] and Mohammad Kassemi[2]
*National Center for Space Exploration Research (NCSER), Case Western Reserve University and NASA Glenn Research Center, Cleveland, OH 44135, USA*
Daniel Hauser[3]
*NASA Glenn Research Center, Cleveland, OH 44135, USA*

**A two-phase CFD model for tank pressurization in a cryogenic storage tank partially filled with liquid hydrogen followed by a sloshing interval is presented using the Volume-of-Fluid approach for capturing the phase boundary and the associated interfacial heat, mass and momentum transfer between the liquid and vapor regions. The CFD model is validated against the pressurization and sloshing data for NASA K-Site tank provided by Moran et al.[1]. Cases with different sloshing amplitudes and frequencies are studied. The results of tank pressurization simulations are presented first followed by the results of the sloshing tests. Predicted tank pressures and temperatures are compared with the experimental data.**

## Nomenclature

| | | |
|---|---|---|
| *AC* | = | accommodation coefficient |
| *E* | = | energy, J |
| F | = | force, N |
| **g** | = | gravitational acceleration, m/s$^2$ |
| *h* | = | enthalpy, J/kg |
| *k* | = | thermal conductivity, W/m·K |
| MT | = | mass transfer |
| mtr | = | mass transfer rate, kg/s |
| ***n*** | = | normal vector |
| *p, P* | = | pressure, Pa |
| *r* | = | surface curvature, m |
| *S* | = | source term |
| *t* | = | time, seconds |
| T | = | temperature, K |
| **v** | = | velocity, m/s |
| VOF | = | Volume of Fluid |

*Greek*

| | | |
|---|---|---|
| $\alpha$ | = | cell value of volume fraction |
| $\mu$ | = | dynamic viscosity, Pa·s |
| $\rho$ | = | density, kg/m$^3$ |
| σ | = | surface tension, N/m |

*Subscripts*

| | | |
|---|---|---|
| *eff* | = | effective |

[1] Research Assistant Professor, Department of Mechanical & Aerospace Engineering, and AIAA Member.
[2] Research Professor, Department of Mechanical & Aerospace Engineering, AIAA Associate Fellow.
[3] Fluids Engineer, Fluid and Cryogenic Systems Branch.

$i$ = interface
$q$ = phase

## I. Introduction

Since the 1960s, NASA's exploration of cryogenic propellant technologies for space propulsion has been pivotal in advancing the efficiency of space vehicles. A primary challenge in this domain is managing volatile cryogenic propellants under the low-gravity conditions of space. Here, the movement of these fluids, known as sloshing, becomes more pronounced, complicating the control of the pressurant used for moving the propellant into storage or for engine use. NASA Glenn and its partners have conducted numerous ground tests to understand these challenges and the required pressurant dynamics. Effectively managing sloshing in propellant tanks is vital for the efficiency of guidance, navigation, and control systems, especially to ensure mission stability and efficiency. When cryogenic propellant tanks are pressurized, gas condensation on the liquid surface can increase the propellant's temperature. Disturbances causing sloshing lead to further condensation and a rise in temperature and pressure, which can be critical during storage or on missions to the Moon or Mars.

Understanding the sloshing behavior of cryogenic propellant in storage tanks is essential for the design of modern rockets that will be used in future NASA missions. Due to the high costs of conducting experiments with cryogenic fluids at different gravitational acceleration levels, it has become advantageous to develop Computational Fluid Dynamics (CFD) models to capture the physical phenomena and assess the fluids and heat transfer performance of the propellant tanks. However, these models must be validated against the experiments to ensure that they can reliably predict the propellant behavior during launch and in the microgravity environment of space.

In orbit, cryogenic propellants face the challenge of heat absorption, leading to an increase in both temperature and pressure within the storage tank. This heat absorption is further intensified by the sloshing of the propellant, a phenomenon more pronounced in microgravity. As a result, to avoid surpassing the safety thresholds of the tank, venting or boiloff processes might be necessary, which unfortunately results in the loss of valuable propellant. According to NASA’s investigations, this sloshing notably escalates the demand for pressurant, significantly influencing the propellant’s average temperature and pressure levels.

Responding to these challenges, NASA is focused on developing and refining CFD models to better comprehend these complex processes, including the intricate heat and mass transfer dynamics involved in condensation and evaporation. These models are rigorously tested against ground experiments to enhance their precision and reliability.

A number of experiments and computational studies were performed to study sloshing behavior and its effect on the cryogenic tank pressure and temperature. Moran et al.[1] studied sloshing in a 62 cubic feet K-Site tank filled with liquid hydrogen. Effects of different parameters on the tank pressure collapse during sloshing were investigated. These parameters include different sloshing frequencies and magnitudes, different tank fill levels and different modes of tank autogenous pressurization prior to sloshing. Himeno et al.[2] at the University of Tokyo experimentally studied sloshing of liquid Nitrogen in a small-scale tank where the effect of liquid stratification on the tank pressure drop was investigated. Konopka et al.[3] experimentally and numerically studied isothermal liquid nitrogen sloshing, non-isothermal draining, and non-isothermal sloshing in a 25 cubic feet tank. Liu et al.[4] computationally studied liquid oxygen sloshing in a 3.5 m diameter tank using the ANSYS Fluent CFD code. In their study reasonable agreement with the experimental data was achieved using Fluent’s built-in phase change model. An important deficiency of this model is that it can predict evaporation/condensation in the bulk liquid and vapor regions based on saturation temperature conditions. Kartuzova et al.[5] developed a CFD model of liquid nitrogen sloshing in a small-scale tank and validated it against the experiment of Himeno et al.[2]. They used kinetic-based Schrage’s relation[6] for calculating the phase change mass transfer at the liquid-vapor interface. They studied the effect of different thicknesses of a liquid temperature stratification layer created at the interface on the pressure drop during sloshing with predictions matching experimental data well. The role of Accommodation Coefficient (AC) used to predict the interfacial mass transfer was also presented and analyzed in their paper.

The literature review indicates that few computational models are validated against cryogenic sloshing in a large-scale tank experiment. This paper contributes to the field by developing a computational model, validated against tank pressurization and sloshing experiments, as reported by Moran et al.[1] in their 1994 study. In this experiment, a 62 cubic foot tank (also known as the K-Site tank) filled with liquid hydrogen and its vapor was used. Test cases 869 and 870 were selected for model validation for their differing sloshing amplitudes and frequencies. The details of the CFD model and validation results are presented, starting with the tank pressurization cases followed by the sloshing

cases. This work aims to fill the gap in computational models validated against large-scale tank experiments in cryogenic sloshing, enhancing the understanding and management of these phenomena in space missions.

## II. Experimental Setup

In the K-Site experiment the aluminum test tank is mounted inside a 25-foot diameter stainless steel vacuum chamber[1]. A sketch of the test tank internals and the instrumentation used for the slosh tests is shown in Fig. 1. Slosh is produced by a shaker mechanism capable of six inches of total displacement at a frequency of one Hertz. The tank lid is constructed of stainless steel, while the remainder of the tank is aluminum. The steady state environmental heat leak into the tank reported by Moran et al.[1] is 0.3 Btu/s. In the experiment a video recording of the internal tank conditions was conducted through the viewing port, which is approximately 60 degrees above the tank midline, and 40 degrees left of the sloshing system's shaft axis, from an observation point directly at the chamber opening. Test tank instrumentation included (see Fig. 1): silicon diodes for temperature sensing on the tank walls; internally thermocouples for fluid stream temperature measurements; pressure transducers; a liquid level probe; vapor-liquid point sensors; and the measured mass flowrate of the pressurant and propellant streams.

For the closed tank slosh tests the test tank is filled to the desired level with either liquid or slush hydrogen, and then vented to approximately 1 atm. The pressurization gas temperature is then preconditioned using the liquid hydrogen and or liquid nitrogen heat exchanger(s). With the temperature of the pressurization gas conditioned, the tank is pressurized with either hydrogen or helium to the desired tank pressure. After stopping the pressurant flow and closing the vent valve, shaking is initiated at the preset frequency, and the amplitude is increased to the desired value. The test amplitude is reached in approximately 10 to 30 seconds. Shaking is maintained for a minimum of two minutes after reaching the desired frequency and amplitude at which time the test is terminated.

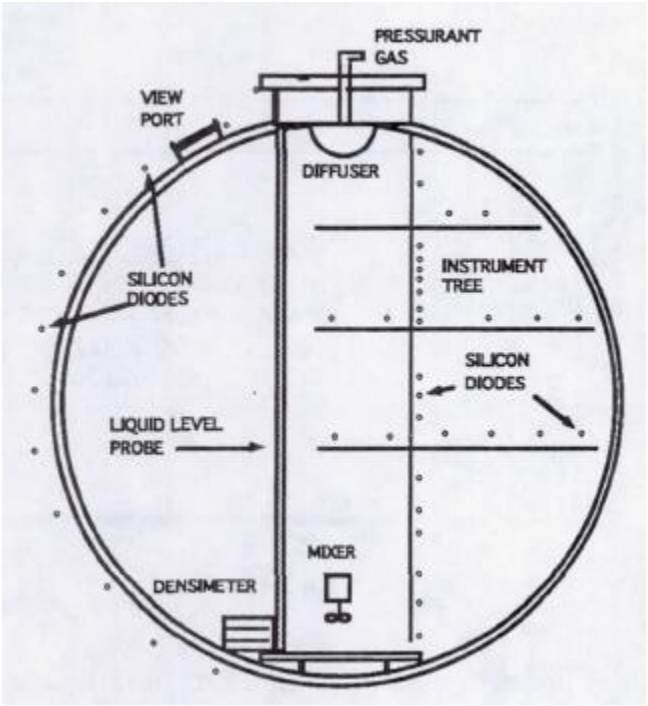


**Figure 1: Schematic of the K-Site tank and instrumentation (Moran et al.[1])**

## III.Mathematical Model

### A. Governing Equations

Fluid flow and heat transfer in the tank are described in terms of the continuity, Navier-Stokes and energy equations for both phases:

$$\frac{\partial \rho}{\partial t} + \nabla(\rho \mathbf{v}) = 0, \tag{1}$$

$$\frac{\partial}{\partial t}(\rho \mathbf{v}) + \nabla(\rho \mathbf{v}\mathbf{v}) = -\nabla p + \nabla\left[\mu_{eff}(\nabla \mathbf{v} + \nabla v^T)\right] + \rho \mathbf{g} + \mathbf{F}_{vol}, \tag{2}$$

$$\frac{\partial}{\partial t}(\rho E) + \nabla\big(\mathbf{v}(\rho E + p)\big) = \nabla\big(k_{eff} \nabla T\big) + S_h. \tag{3}$$

In the present study, the liquid phase is treated as incompressible with variable temperature-dependent properties, except for density. The liquid density is allowed to vary linearly with temperature in the body force term of the momentum equation according to the Boussinesq approximation. The vapor is modeled as a compressible ideal gas. In this study, the movement of the interface is captured diffusely using the Volume of Fluid (VOF) method, as promogulated by Hirt and Nichols[7]. Interfacial energy, momentum and mass balances are applied using source terms in the diffuse interfacial region.

**B. VOF Model**

In the VOF method, a volume fraction is defined in each cell such that the volume fractions of all the phases sum to unity. In the cell, the change in the interface can be tracked by solving a continuity equation for the volume fraction of the $q^{th}$ phase:

$$\frac{1}{\rho_q}\left[\frac{\partial}{\partial t}(\alpha_q \rho_q) + \nabla \cdot (\alpha_q \rho_q \mathbf{v}_q) = S_{\alpha_q}\right], \tag{4}$$

where the volume fraction for the primary phase is determined from:

$$\sum_{q=1}^{n} \alpha_q = 1. \tag{5}$$

In the VOF method, the field variables and properties are defined in terms of the volume fraction, which for a general system can be written as:

$$\rho = \sum_{q=1}^{n} \alpha_q \rho_q, \qquad \mu_{eff} = \sum_{q=1}^{n} \alpha_q \mu_{eff_q}, \qquad k_{eff} = \sum_{q=1}^{n} \alpha_q k_{eff_q}. \tag{6}$$

In this fashion, the continuity, momentum and energy equations, as described by Eq. (1) – (3), can be solved throughout the domain for the temperatures and velocities in the two phases. In the VOF model, energy ($E$) and temperature ($T$) are treated as mass-averaged variables:

$$E = \frac{\sum_{q=1}^{n} \alpha_q \rho_q E_q}{\sum_{q=1}^{n} \alpha_q \rho_q}, \tag{7}$$

where $E_q$ is based on the specific heat of the $q^{th}$ phase and the shared temperature.

Evaporation and condensation at the interface are modeled as a source term in the continuity equation for the volume fraction (Eq. 4), i.e.:

$$S_{\alpha_q} = \dot{\mathbf{m}}_i \cdot \mathbf{A}_i\,, \tag{8}$$

where $\mathbf{A}_i$ is an interfacial area density vector, and $\dot{\mathbf{m}}_i$ is a mass flux vector, which for near equilibrium conditions can be determined based on the Schrage[3] equation:

$$|\dot{\mathbf{m}}| = \left(\frac{2\sigma}{2-\sigma}\right)\left(\frac{M}{2\pi R}\right)^{1/2}\left(\frac{P_i}{T_i^{1/2}} - \frac{P_v}{T_v^{1/2}}\right). \tag{9}$$

Here $\sigma$ is the accommodation coefficient; $M$ is the molar mass of the fluid; $R$ is the universal gas constant; $P_i$ and $P_v$ are, respectively, the interfacial and vapor pressures (it was assumed that $P_i \cong P_{sat}$); $T_i$ and $T_v$ are, respectively, the interfacial and vapor temperatures (it was assumed that $T_i = T_v \cong T_{sat}$ at the interface). Finally, $\mathbf{A}_\mathbf{i}$ is defined as:

$$\mathbf{A}_i = |\nabla \alpha|, \tag{10}$$

where $\alpha$ is the volume fraction of the primary phase.

In the present implementation, the surface tension forces at the interface are modeled via the Continuum Surface Force (CSF) model of Brackbill et al.[8]. In this model, the surface tension forces at the interface are transformed into a volume force ($\mathbf{F}_{vol}$), which is added as a source to the momentum equation:

$$\mathbf{F}_{vol} = \sum_{pairs\ ij, i<j} \sigma_{ij} \frac{\alpha_i \rho_i h_i \nabla \alpha_j + \alpha_j \rho_j h_j \nabla \alpha_i}{\frac{1}{2}(\rho_i + \rho_j)}\,, \tag{11}$$

where $h_i$ is the surface curvature calculated from the local gradients in the surface normal at the interface:

$$h_i = \nabla \cdot \hat{\mathbf{n}}. \tag{12}$$

### C. Turbulence modeling

*Large Eddie Simulation (LES)* approach to turbulence modeling was compared with the *Laminar* approach in this study.

In the LES model, large eddies are resolved directly while small eddies are modeled. In the current LES model, the Wall-Adapting Local Eddy-Viscosity (WALE)[9] sub-grid scale model is utilized for modeling the unknown stresses that result from the filtering operation.

## IV. Numerical Implementation

In CFD, just as in the experiment, tank pressurization simulation is performed first. The pressurization is done through a diffuser located at the top of the tank, as shown Figure 1. After the tank pressure reaches a desired value, the incoming gas mass flow rate is significantly reduced to keep the pressure in the tank constant. This is called the "hold" period in the experiment. After the "hold" period, sloshing is initiated, and the tank pressure decreases due to condensation at the interface. During the sloshing, the gas mass flow rate is reduced to 0. Test cases 869 and 870 were selected for model validation. These cases have similar tank pressurization parameters but differ in the sloshing amplitude and frequency. In the case 869, a sloshing frequency of 0.95 Hz and an amplitude of ±0.5 in (±12.7 mm) were applied. In the case 870, a sloshing frequency of 0.75 Hz and an amplitude of ±1.5 in (±38.1 mm) were used.

### D. Tank Geometry

A 1.79 m diameter K-Site tank was considered for model validation. A schematic of the tank is shown in Figure 2. Full 3D tank geometry was used in calculations.

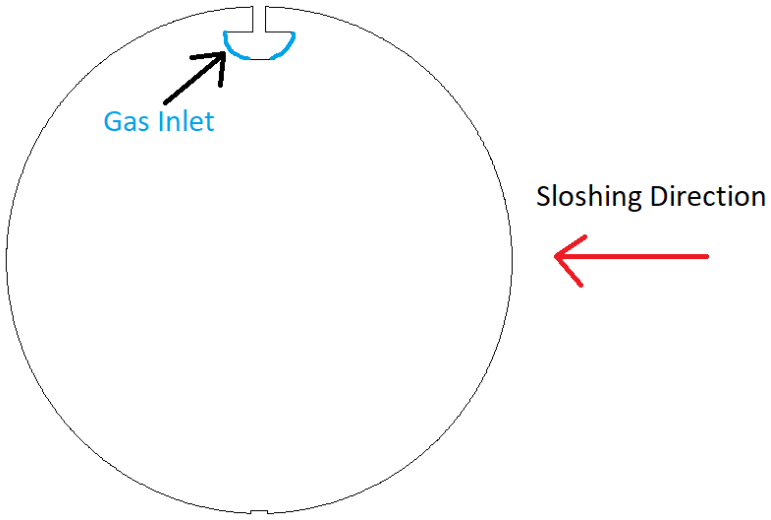


**Figure 2: Tank Geometry used in CFD**

### E. Initial Conditions

In this case initial tank pressure was set to the experimental value for case 870, as reported in Table 1. Liquid temperatures were set to saturation values at the initial tank pressure. The measured initial ullage temperature profile reported by Moran et al.[1] for the case 870 was applied to the vapor domain in both cases. The initial ullage volume was set to the corresponding experimental value for case 870, as reported in Table 1. Only one pressurization case was completed, and its results were used as initial conditions for sloshing for both cases. This assumption was made since the tank pressures at the end of pressurization (ramp) were similar in the experiment.

**Table 1: Test Parameters**

| *Case #* | *Ullage Volume, %* | *Initial Pressure, psia* | *Ramp Pressure, psia* | *Ramp Time, s* | *Ramp Pressurant Added, lbm* | *Hold Time, s* | *Total Pressurant Added, lbm* | *Pressurant Temperature, °R* |
|---|---|---|---|---|---|---|---|---|
| *869* | 33 | 15.4 | 35.4 | 13 | 0.625 | 28 | 0.816 | 71 |
| *870* | 36 | 14.6 | 35.5 | 14 | 0.634 | 27 | 0.813 | 74 |

### F. Boundary Conditions

Conjugated heat transfer through the aluminum tank wall is included in the CFD model. The contact angle between liquid and the tank wall is assumed to be 0 degrees. Non-Slip boundary conditions are applied on the inside of the tank wall which is in contact with the fluid. Gaseous $H_2$ is injected at the gas inlet, as shown in Figure 2. During pressurization measured values of the gas mass flow rate are used. The constant experimental gas temperature as listed in Table 1 is applied uniformly at the gas inlet for each test case. During sloshing, gas injection is turned off. Direction of acceleration applied during the sloshing tests is shown in Figure 2.

### G. Material Properties

Liquid hydrogen and its vapor fill the tank. Parahydrogen properties from NIST REFPROP database were used. Constant saturation properties at the initial tank pressure for each case were used, except for the specific heat, the thermal conductivity, and the viscosity in the vapor, that varied with temperature.

### H. Discretization and convergence

The Second Order Upwind scheme was used to discretize the turbulence, energy, and momentum equations (cell values). The PISO scheme was used for the pressure-velocity coupling (cell values). The Least Squares Cell Based scheme was used for the gradient calculations (face values). The PRESTO! scheme was used for the pressure interpolation (face values). The Point Implicit (Gauss-Seidel) linear equation solver with the Algebraic Multi-Grid (AMG) method were used to solve the linearized systems of equations. The First Order Implicit temporal discretization and the Geometric Reconstruction scheme for the VOF equation was used with the explicit VOF model. The convergence criteria are set to $1x10^{-4}$ for all the equations except the energy equation, for which it is set to $1x10^{-6}$. A time step size value of 0.04 seconds was used during pressurization and a value of 0.001 seconds was used during the sloshing.

### I. Computational mesh

A midplane of the 3D computational grid used in the current study is shown in Figure 3. Polyhedral mesh with refinement near tank walls, but otherwise uniform in size, is used. The mesh size is 3.8 million cells.

In this section the results of CFD simulations are presented and compared with the data obtained in the experiment. Results for tank autogenous pressurization are presented first followed by the results of sloshing cases.

### J. Tank pressurization

Predicted tank pressure during pressurization is presented and compared with the experimental data for case 870 in Figure 4. CFD results are in a good agreement with the measured values during both ramp (pressure increase) and hold (constant pressure) portions of the test. The predicted phase change rate in the tank during like-gas pressurization is shown in Figure 5. Condensation is predicted during the entire pressurization period. Initial temperatures in the tank and temperatures predicted at the end of ramp were compared to their experimental counterparts for case 870. Initial temperatures in the tank are the same in CFD and experiment because experimental values were used as initial conditions in the simulations. Both the CFD simulations and the experiment results show that liquid temperatures remain almost unchanged at the end of the ramp, but the vapor temperatures increase, especially, in the mid-vapor region and near the interface. Predicted temperatures at the top of the vapor region are higher than in the experiment, which is possibly due to extrapolation of temperatures at the top of the tank in CFD that resulted in higher initial temperatures in comparison to the experiment in this region. Figure 7 compares mass flow rate of gas that is added for pressurization together with the condensation rate at the interface. It is clear that during the ramp portion of the test, when the rate of pressurization is high, condensation rate at the interface is small relative to the amount of added gas. However, during the hold portion of the test most of the gas added to the tank condenses at the interface, resulting in a constant tank pressure. Temperature contours at the center plane of the tank,

shown in Figure 8 at the beginning and end of pressurization, show an increase in the vapor temperatures in the middle of the vapor region and near the interface.

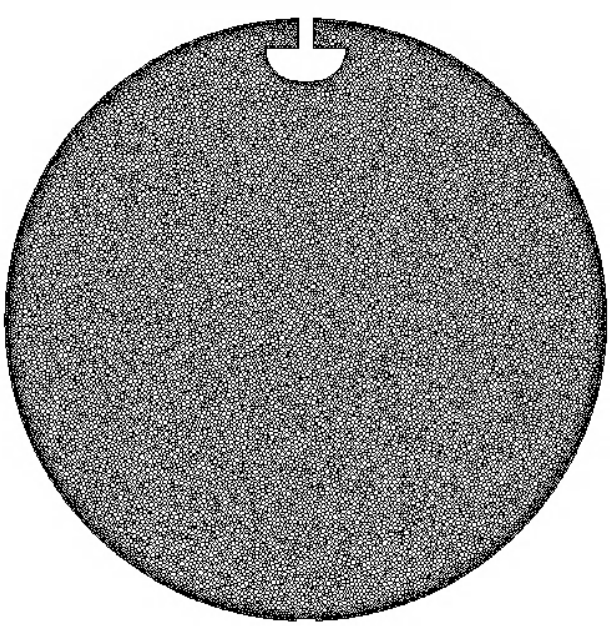

**Figure 3: Computational Mesh**

## V. Results and Discussion

Overall predicted pressure and temperatures in the tank during pressurization portion of the test match experimentally measured values well. CFD results at the end of pressurization are used as initial conditions for sloshing for both test cases 870 and 869, since pressurization portions of both tests were very similar.

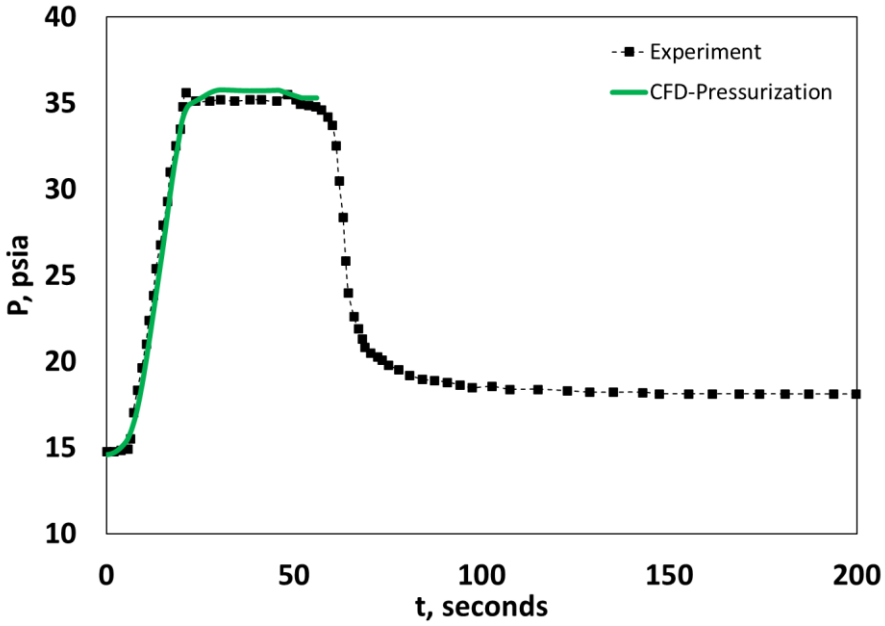


**Figure 4: Tank pressure during like-gas pressurization: CFD vs. Experiment**

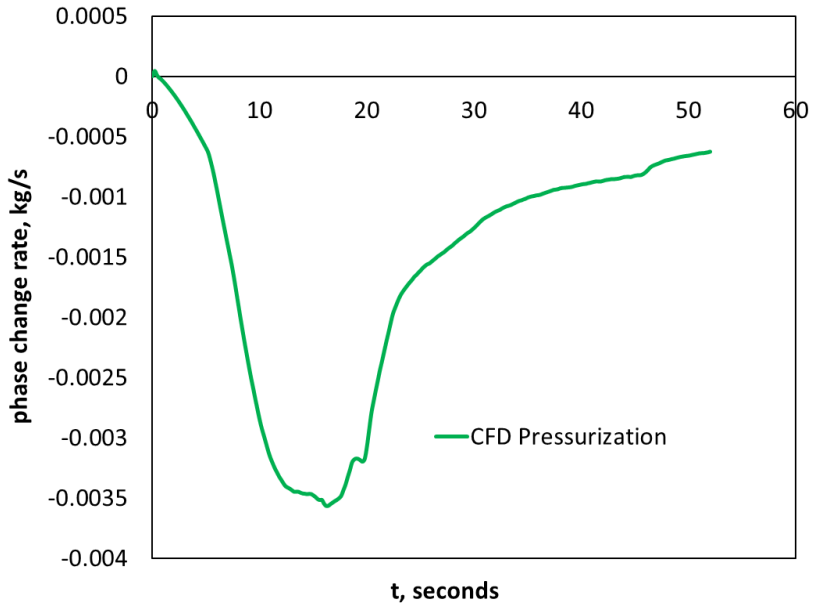


**Figure 5: Predicted phase change rate in the tank during like-gas pressurization**

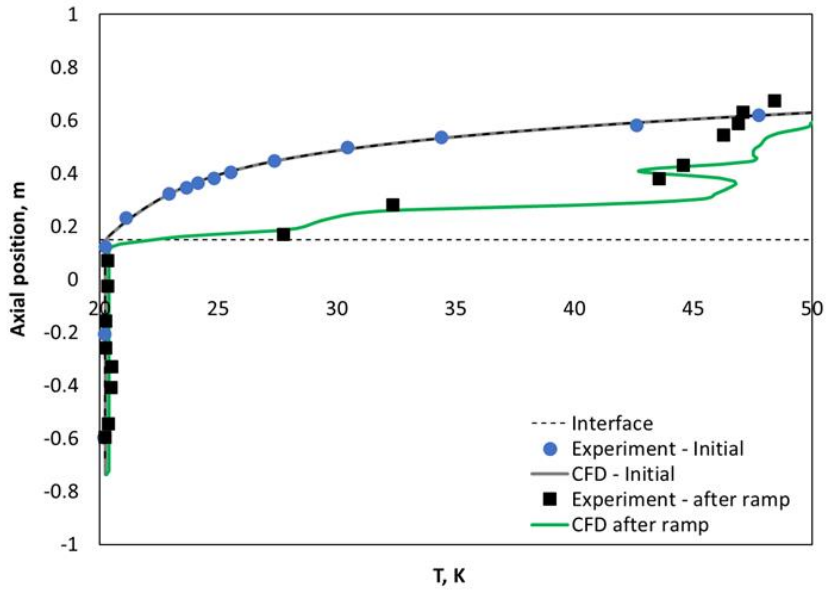


**Figure 6: Initial temperatures in the tank and values predicted at the end of ramp compared to the experimental data**

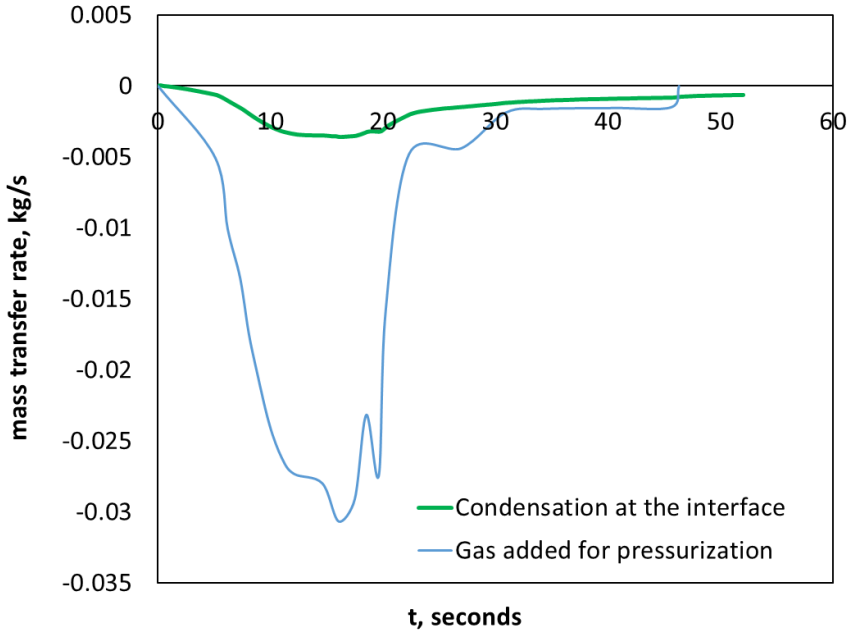


**Figure 7: Predicted phase change rate vs. mass flow rate of gas added during pressurization**

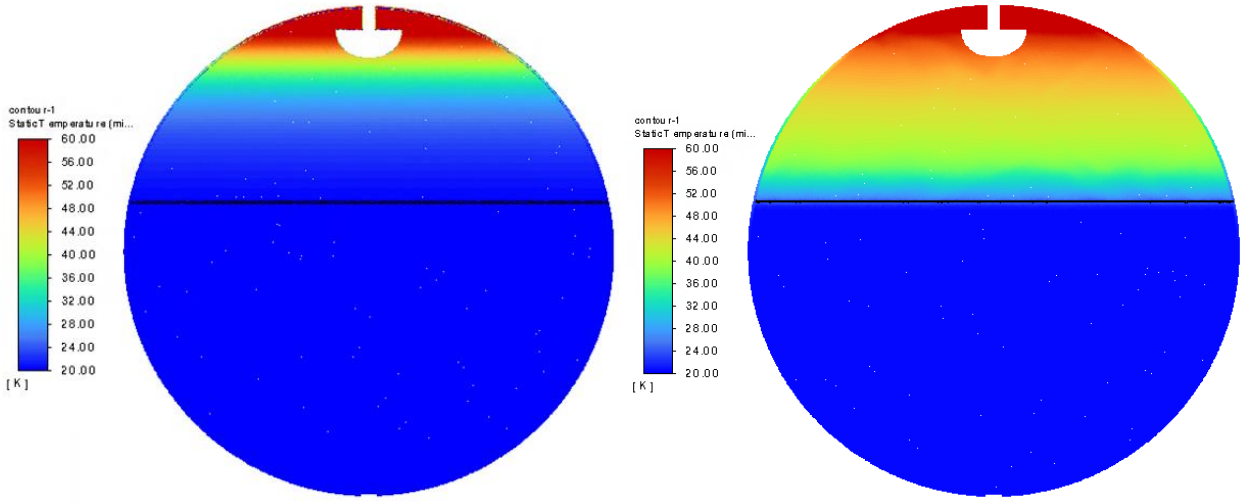


**a) beginning of pressurization** **b) end of pressurization**

**Figure 8: Temperature contours at the center plane of the tank at the beginning (a) and end (b) of pressurization.**

### K. Sloshing

In this section CFD results for sloshing test cases 869 and 870 are presented and discussed. The measured and predicted pressures in the tank during sloshing in cases 869 and 870 are compared in Figure 9. In test case 869, pressure in the tank decreases slowly in both the CFD simulations and the experiment, compared to the results of the test case 870, where it drops quickly after sloshing starts. In both cases predicted tank pressures are in a good agreement with the experimental data and the trend of the tank pressure behavior with respect to sloshing parameters is successfully reproduced. It should be noted here that the test case 870 was completed without phase change (dark blue line in Figure 9). Convergence difficulties prevented from completing this case with phase change due to vigorous interface motion and the significant interface breakup during sloshing with a high amplitude. However, the simulation

cases with phase change that were completed for the first 4 seconds of sloshing (before the onset of convergence issues) with the laminar and LES turbulence models, predict a pressure drop in the tank that is very similar to the results of the model without phase change and experimental data. This suggests that phase change at the interface in this case has a secondary role compared to the effect of heat transfer enhanced by the vigorous movement of the interface. It is important to note here that however the single-phase heat transfer reduced the tank's pressure to the saturation pressure of the liquid, thereby making phase change less relevant in this this case; in the cases where the tank is continuously pressurized, such as during the expulsion tests, vapor condensation into the liquid becomes a significant factor and can't be ignored.

Phase change rates at the interface predicted during sloshing for test cases 870 and 869 are shown in Figure 10. Condensation rates predicted by the laminar model match for both cases during the first 2 seconds of sloshing. After this time, predicted condensation rate increases dramatically in test case 870, but remains relatively constant in test case 869. Both laminar and LES turbulence models predict similar condensation rates during first 4 seconds of sloshing, after this time both cases experience convergence difficulties. Temperature contours at the center plane of the tank and three-dimensional surfaces of the liquid-vapor interface are compared between test cases 870 and 869 at 0, 1, 2, 3, 4, 5 and 50 seconds of sloshing in Figure 11. At 0 and 1 seconds, both the temperatures and the interface surfaces look very similar between the 2 cases. However, at two seconds of sloshing, a larger wave is already predicted in test case 870, compared to the test case 869. At 3 seconds of sloshing, this wave moves to the other side of the tank and falls onto itself, mixing the vapor, in test case 870. At the same time, in test case 869, no waves are created at the interface. At four and five seconds of sloshing, vigorous movement of the interface and extensive mixing of the vapor region is predicted in test case 870. In test case 869, very little interface motion leaves the vapor region virtually unmixed, and it remains unmixed after 50 seconds of sloshing and until the end of the sloshing period (not shown here). In test case 870, the vapor continues to become well-mixed after 50 seconds of sloshing with large waves and significant interface breakups present.

The Slosh stability map for the test cases 869 and 870 is shown in Figure 12. This map indicates stable and unstable sloshing regions based on the sloshing frequency and amplitude. It is clear that test case 869 is in the stable region and test case 870 is well within the unstable sloshing region. CFD results presented earlier lead to the same conclusion and illustrate the effect of sloshing stability on tank pressure and temperatures.

## VI. Conclusion

A computational model of K-Site tank pressurization with gaseous Hydrogen followed by sloshing at different frequencies and amplitudes has been developed and its predictions were compared with the experimental data presented by Moran et al.[1]. The CFD model was first applied to simulate tank autogenous pressurization and then to model experimental sloshing test cases 869 and 870. These cases have similar tank pressurization parameters but differ in sloshing amplitude and frequency. In this study an in-house developed VOF phase change model was utilized to predict heat and mass transfer at the interface.

During autogenous pressurization tank pressure increased quickly to the desired value and then stayed constant in response to the amount of incoming pressurant gas, balancing condensation at the interface. Predicted tank pressures match measured values very well.

Sloshing simulations followed pressurization simulations. Here two different cases were considered. In the test case 869, a sloshing frequency of 0.95 Hz and an amplitude of ±0.5 in (±12.7 mm) were applied resulting in a moderate amount of sloshing and a slight pressure decrease in the tank. In the test case 870, a sloshing frequency of 0.75 Hz and an amplitude of ±1.5 in (±38.1 mm) were applied resulting in violent sloshing with enhanced mixing of the vapor region and a sharp pressure drop in the tank. In this case, convergence difficulties prevented completing the case with phase change at the interface. However, simulating 4 seconds of sloshing with phase change, revealed very little effect of phase change on the tank pressure when compared to the results of the case without phase change. This led to conclusion that phase change is of a lesser importance in the case where violent sloshing promotes mixing and enhances heat transfer in the vapor region. Predicted tank pressures for both cases are in a good agreement with the experimental data, confirming the experimental trends.

A slosh stability map was also created. It indicates that test case 870 falls in an unstable sloshing region while test case 869 is well in the stable region. This is in line with CFD results. Validation of the current CFD model against K-Site Hydrogen sloshing experiments, demonstrated its ability to accurately capture effects of sloshing on the tank pressure at widely different sloshing frequencies and amplitudes.

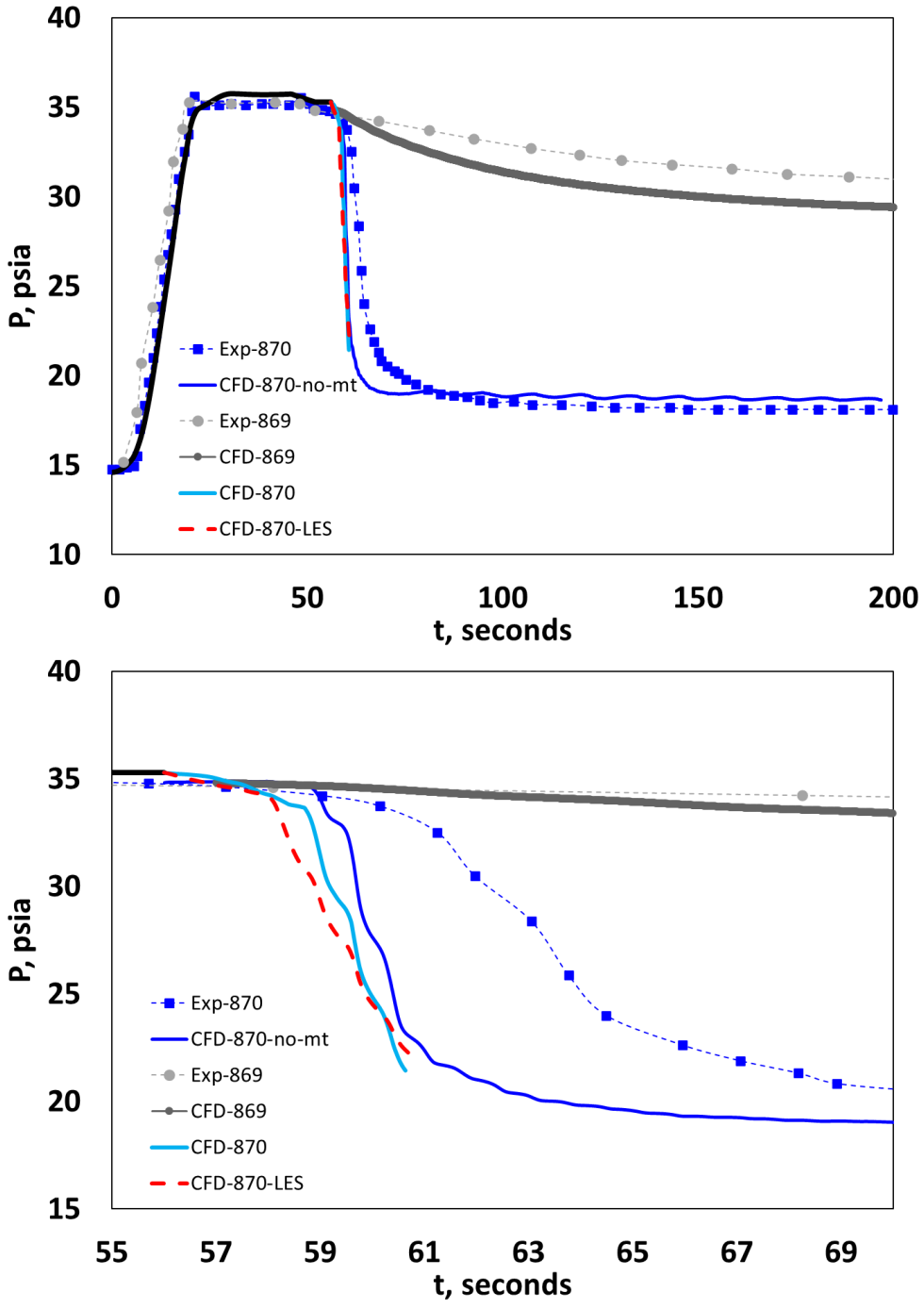


**Figure 9: Tank pressure during sloshing after like-gas pressurization: CFD vs. Experiment**

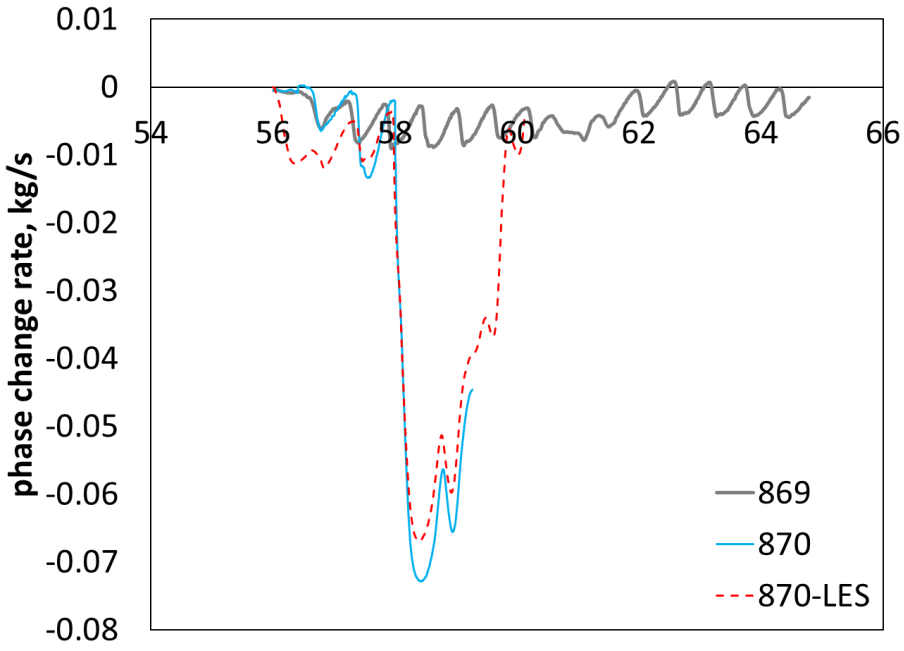


**Figure 10: Comparison of the phase change rate at the interface during sloshing for cases 870 and 869.**

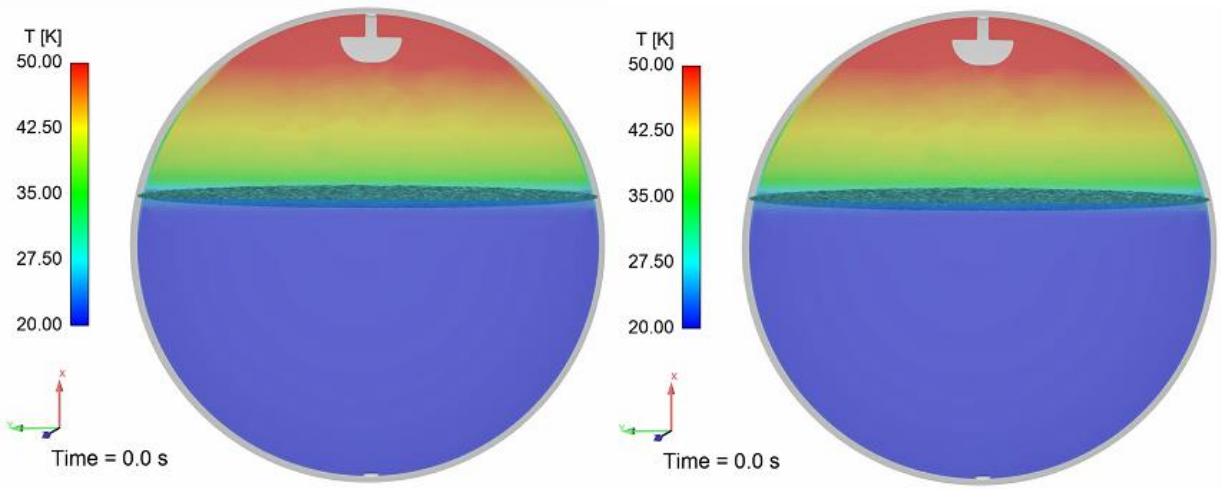


**870** **869**

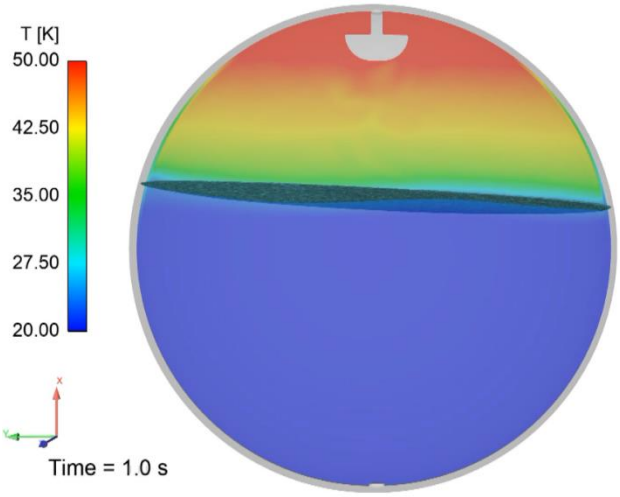


**870**

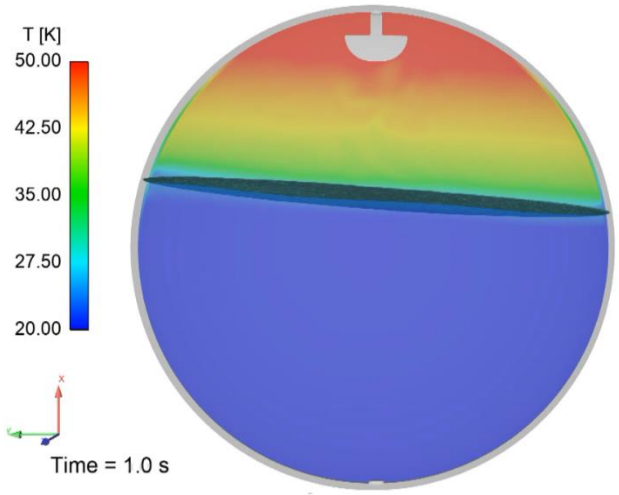


**869**

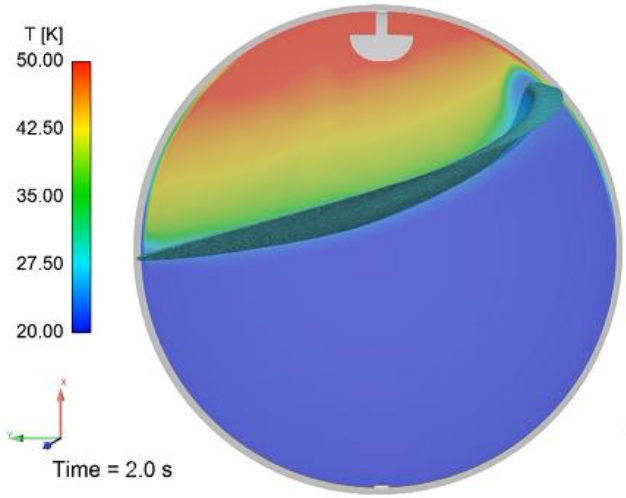


**870**

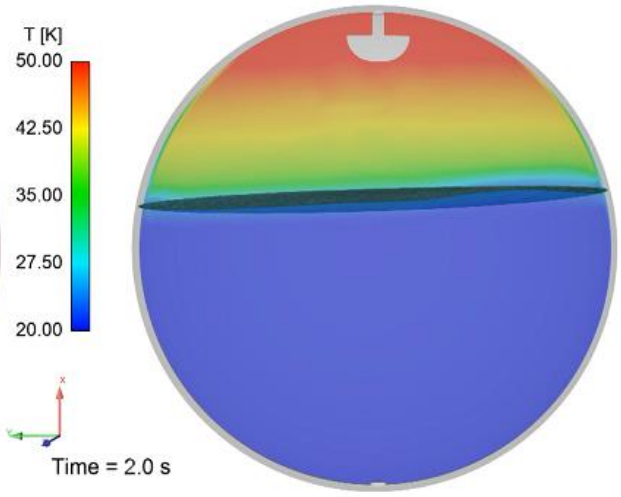


**869**

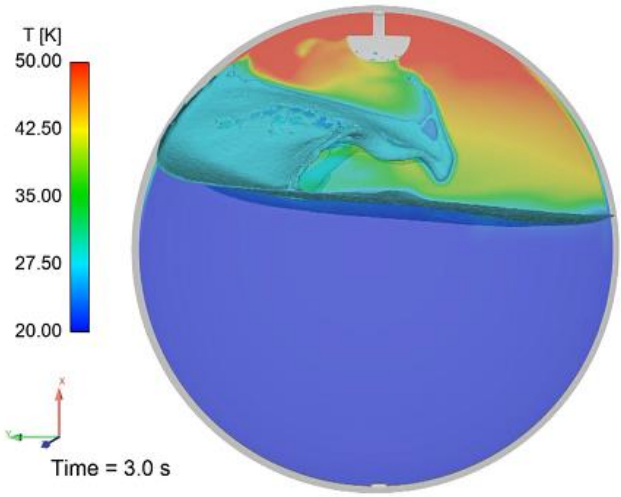


**870**

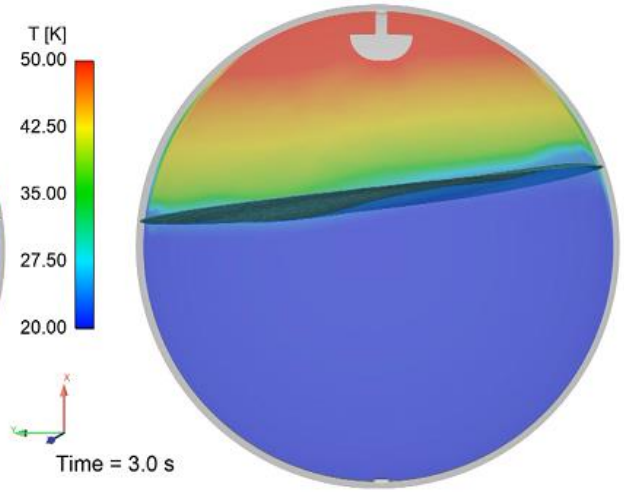


**869**

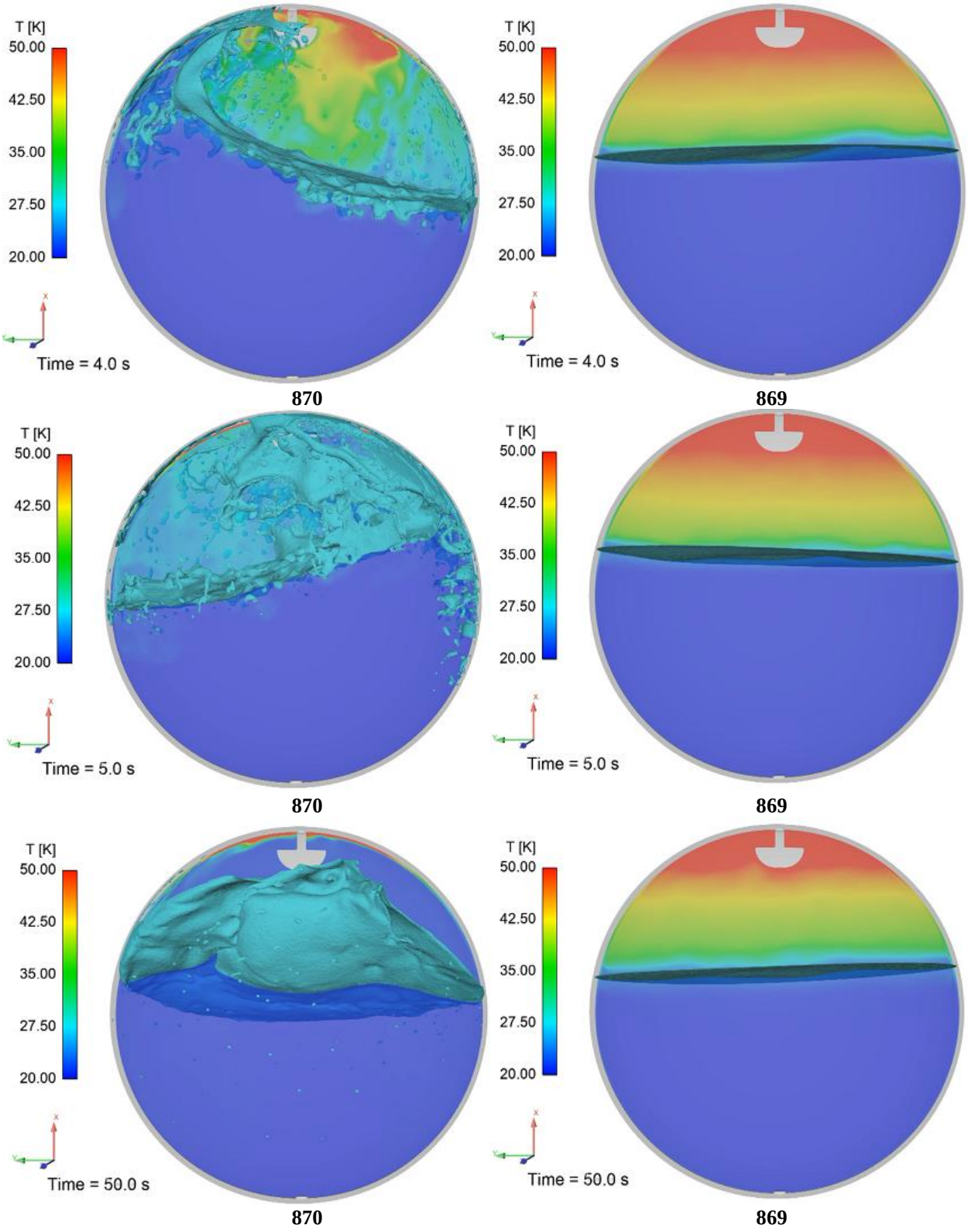


**Figure 11: Temperature contours at the center plane of the tank and the 3D interface surface at different times during sloshing for cases 870 and 869**

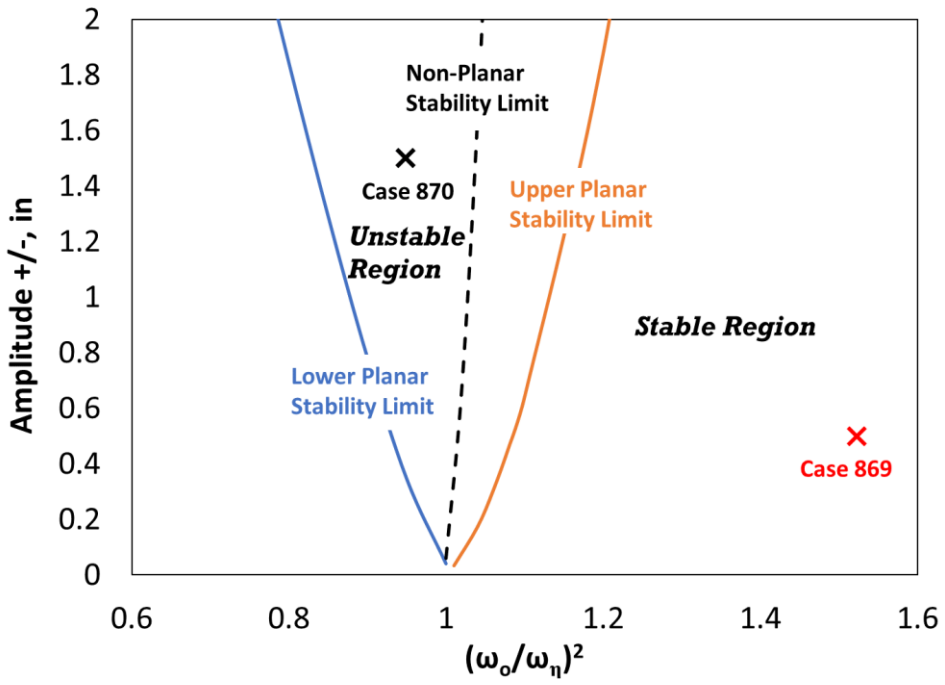


**Figure 12: Slosh stability map for cases 869 and 870**

## Acknowledgments

Authors would like to thank Michael Baker (HX5) for providing tank and diffuser geometry; and the Modeling Portfolio Project within the STMD CFM Project Office for providing funding for this work.

## References

[1] Moran, M.E., McNelis, N.B., Kudlac, M.T., Haberbusch, M.S., Satorino, G.A. "Experimental Results of Hydrogen Slosh in a 62 Cubic Foot (1750 Liter) Tank," NASA TM-106625, 1994

[2] Himeno, T., et al., "Investigation on Phase Change and Pressure Drop Enhanced by Violent Sloshing of Cryogenic Fluid", AIAA Propulsion and Energy Forum, July 2018, Cincinnati, OH, AIAA 2018-4755

[3] Konopka, M., Noeding, P., Klatte, J., Behruzi, P., Gerstmann, J., Stark, A., and Darkow, N. "Analysis of LN2 filling, draining, stratification and sloshing experiments." In 46th AIAA fluid dynamics conference, p. 4272. 2016.

[4] Liu, Z., Cai, H., Feng, Y., Liu, Y., Li, Y. "Thermodynamic characteristic in a cryogenic storage tank under an intermittent sloshing excitation", International Journal of Hydrogen Energy, Volume 45, Issue 21, 2020, pp. 12082-12094.

[5] Kartuzova O., Kassemi, M., Umemura Y., Kinefuchi K., and Himeno T. "CFD Modeling of Phase Change and Pressure Drop during Violent Sloshing of Cryogenic Fluid in a Small-Scale Tank", AIAA Propulsion and Energy Forum, August 2020, Virtual, AIAA 2020-3794.

[6] Schrage, R.W. A theoretical study of interphase mass transfer, Columbia University Press, New York, 1953.

[7] Hirt, C.W., and Nichols, B.D. "Volume of fluid (VOF) method for the dynamics of free boundaries", Journal of Computational Physics 39 (1): 201-225. 1981.

[8] Brackbill J.U., Kothe, D.B., Zemach, C., "A continuum method for modeling surface tension," J. Comp. Phys. Vol. 100, 1992, pp. 335–354.

[9] ANSYS Fluent 2023 R1 Documentation